ACS APPLIED MATERIALS & INTERFACES

Research Article

Cite This: ACS Appl. Mater. Interfaces 2018, 10, 33589−33600

www.acsami.org

Role of Filler Porosity and Filler/Polymer Interface Volume in Metal−Organic Framework/Polymer Mixed-Matrix Membranes for Gas Separation

Alexander Nuhnen, Dennis Dietrich, Simon Millan, and Christoph Janiak*

Institut für Anorganische Chemie und Strukturchemie, Heinrich-Heine-Universität, Universitätsstraße 1, D-40225 Düsseldorf, Germany

Supporting Information

ABSTRACT: Metal−organic frameworks (MOFs) and inorganic fillers are frequently incorporated into mixed-matrix membranes (MMMs) to overcome the traditional trade-off in permeability (P) and selectivity for pure organic polymer membranes. Therefore, it is of great interest to examine the influence of porous and nonporous fillers in MMMs with respect to the possible role of the polymer−filler interface, that is, the void volume. In this work, we compare the same MOF filler in a porous and nonporous state, so that artifacts from a different polymer−filler interface are excluded. MMMs with the porous MOF aluminum fumarate (Al-fum) and with a nonporous dimethyl sulfoxide solvent-filled aluminum fumarate (Al-fum(DMSO)), both with Matrimid as polymer, were prepared. Filler contents ranged from 4 to 24 wt %. Gas separation performances of both MMMs were studied by mixed gas measurements using a binary mixture of CO_2/CH_4 with gas permeation following the theoretical prediction by the Maxwell model for both porous and nonporous dispersed phase (filler). MMMs with the porous Al-fum filler showed increased CO_2 and CH_4 permeability with a moderate rise in selectivity upon increasing filler fraction. The MMMs with the nonporous Al-fum(DMSO) filler displayed a reduction in permeability while maintaining the selectivity of the neat polymer. A linear dependence of log P versus the reciprocal specific free fractional volume (sFFV) rules out a significant contribution from a void volume. The sFFV includes the free volume of the polymer and the MOF, but not the polymer−filler interface volume (so-called void volume). The sFFV for the MMM was calculated between 0.23 cm^3/g for a 24 wt % Al-fum/Matrimid MMM and 0.12 cm^3/g for a 24 wt % Al-fum(DMSO)/Matrimid MMM. The negligible effect of an interface volume is supported by a good matching of theoretical and experimental density of the Al-fum and Al-fum/(DMSO) MMMs which gave a specific void volume below 0.02 cm^3/g, often even below 0.01 cm^3/g.

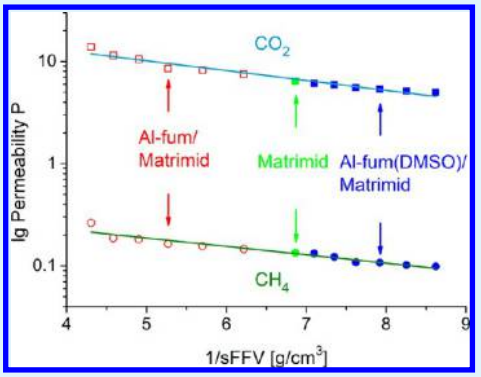

KEYWORDS: *MOFs, metal−organic frameworks, Matrimid, mixed-matrix membrane, nonporous filler, free fractional volume, void volume, gas separation*

INTRODUCTION

Membrane science and technology has attracted continuous attention over the last few decades due to its superior separation properties in comparison to conventional methods, such as crystallization, distillation, or adsorption processes.[1−3] Since purification processes based on membranes feature high energy efficiency, low production costs, and simple process conditions, they are very attractive for industrial application.[4,5]

Gas separation efficiency through dense polymer membranes is generated through a unique separation process as no high energy phase transformation is needed, unlike in the conventional separation processes. Separation through membranes is dependent instead on size, shape, and interaction of the molecules with the membrane material.[6] Membranes therefore can be characterized by two main properties to determine their efficiency. The permeability describes the velocity in which the gases travel through the membrane, and the selectivity exhibits the separation potential between two or more gases.[7]

At the current state low flux polymeric membranes are widely used in industrial processes because of their high flexibility, easy processing, low costs, and mechanical strength.[8] Yet, polymeric membranes display a major disadvantage since they exhibit an inverse relation, a trade-off between high gas permeation or good selectivity.[9] This inverse relation between permeation and selectivity is illustrated in the so-called Robeson upper bound.[9,10] A possible way to overcome this trade-off is realized by embedding inorganic or organic−inorganic hybrid materials as fillers into the polymer matrix to receive mixed-matrix membranes (MMMs).[11−14]

Received: July 30, 2018
Accepted: September 7, 2018
Published: September 7, 2018

DOI: 10.1021/acsami.8b12938
ACS Appl. Mater. Interfaces 2018, 10, 33589−33600

The used fillers can generally be divided into two groups: porous and nonporous fillers. In the field of porous fillers zeolites and highly porous metal organic frameworks (MOFs) are the most studied materials in MMMs.[15−17] Because of their high tuneability and structural diversity MOFs can be customized for different polymer matrices to obtain micro-defect free MMMs or enhance their separation properties.[18,19] Usually it is found that the permeability of defect free MMMs increases with the loading of the MOF and the selectivity remains unaltered or raises only in a moderate way in comparison to the neat polymer.[20] The increase of permeability is either associated with the porous nature of the MOFs, which therefore increases the free fractional volume (FFV) of the MMMs, or to the presence of isolated voids in the interface between the MOF and the polymer.[21,22] Free fractional volume refers to the inherent porosity within the polymer and the porous filler, here the MOF. The FFV does not include any voids formed around the filler particles due to phase incompatibility. However, a consequence of voids, which become connected through a membrane because of high filler loading, will be that these MMMs show an increased permeability and a partial or complete loss of selectivity as such connected voids would be nonselective.[23,24]

Exemplary for this behavior Basu et al. studied the permeation properties of MIL-53(Al)/Matrimid, Cu-BTC/Matrimid, and ZIF-8/Matrimid MMMs for CO_2 and CH_4 and found a continuous increase in CO_2 and CH_4 permeation with growing amount of MOF. Thereby CO_2 permeation enhancement was slightly higher in relation to CH_4, resulting in a moderate rise of their selectivity.[25] A way to enhance the selectivity in a significant manner was specified by Zornoza et al., using the amino modified NH_2-MIL-53(Al) embedded in a polysulfone matrix.[13] The characterization of the MMMs showed a doubling in selectivity for the MMMs with 25 wt % MOF including a minor raise in CO_2 permeability, before losing their separation properties with higher loadings up to 40 wt % MOF.

Studies of nonporous fillers in MMMs mostly focus on nanoparticles based on fumed silica or other oxides.[14,26] As nonporous fillers are not permeable for gases, they should lower the permeability of the MMMs with increasing amount of the filler, as long as one obtains an ideal MMM. This behavior was shown by Sadeghi et al. when they incorporated silica nanoparticles into a polyether polymer matrix. The MMMs show a reduction of permeability for several gases with increasing amount of silica.[27] Nevertheless Merkel et al., Ahn et al., and Ahmadpour et al. experienced an increase of the permeability for their MMMs with nonporous nanoparticles in comparison to the neat polymer.[14,26,28] Ahn et al. explained the rise in permeability as a result of interfacial voids between nanoparticles and polymer. They quantified the resulting voids by comparing the actual density of the MMMs with the theoretically calculated density and could therefore determine the void volume of the MMMs.[28] The interfacial voids were associated with poor interactions of the inorganic nanoparticles with the polymer phase.[29] With porous fillers the determination of interfacial voids is rarely done. It was shown that there is a correlating increase between FFV and permeability, but no such correlation could be seen between void volume and permeability.[21]

With porous fillers an increase in permeability is seen as normal and viewed as an expected property. However, it cannot automatically be deduced that this increase is due to the porosity of the filler. With the formation of interfacial voids, such an increase could also derive therefrom.[23,24]

To the best of our knowledge, the relative role of porosity in the filler and interfacial voids between filler and polymer have not been clearly elucidated. Understandably it is not straightforward to conceive how the chemically same filler material could be prepared in a porous and nonporous way. Therefore, we prepared for the first time (to the best of our knowledge) a porous and a nonporous filler based on the same MOF, with the same properties as particle size, structure, and interaction with the polymer, only differing in their porosity. By embedding both fillers in the polymer Matrimid one should see which influence porosity and interfacial voids have, respectively. If the void volume is responsible for a higher permeability in MMMs, compared to the neat polymer, then one would expect a rise in permeability for both kinds of filler. If, however, the porosity is responsible for an increase in permeability, then one would expect a rise in permeability only for the MMMs with the porous filler.

RESULTS AND DISCUSSION

Al-fum and Al-fum(DMSO) Characterization. In this study the properties of porous and nonporous fillers in MMMs, based on the MOF aluminum fumarate as filler and Matrimid as polymer, is examined. Aluminum fumarate (Al-fum) was synthesized according to a recently described procedure which yields submicrometre particles of the MOF.[30] Particle size and morphology of fillers have great influence on the distribution of MOF particles in the polymer matrix. Thus, they affect phenomena such as sedimentation and agglomeration of the filler and ultimately reduce or increase microdefects in MMMs which affects permeation results.[13,31,32] Here, the obtained Al-fum particles had a size of about 250 nm, characterized by SEM (Figure S2 of the Supporting Information, SI), which is in good agreement with the literature.[30] Furthermore, the successful synthesis of aluminum fumarate was shown by a positive matching of the experimental PXRD to the simulated pattern (Figure 1). The synthesis of aluminum fumarate-(DMSO) (Al-fum(DMSO)), that is, pore filling of Al-fum by dimethyl sulfoxide, was achieved by stirring Al-fum in dimethyl sulfoxide at 180 °C overnight. DMSO-filling did neither alter the Al-fum particle size of about 250 nm (Figure S2) nor the crystallinity (Figure 1). The PXRD in Figure 1 shows slightly

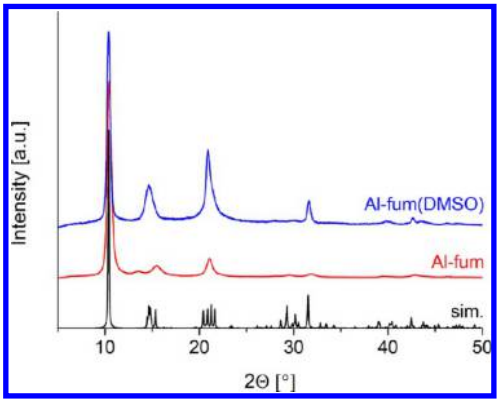

Figure 1. Powder X-ray diffractograms for Al-fum in red and Al-fum(DMSO) in blue in comparison with the simulated diffractogram (sim., based on the X-ray data refinement, CCDC number: 1051975)[37] in black.

DOI: 10.1021/acsami.8b12938
ACS Appl. Mater. Interfaces 2018, 10, 33589−33600

higher intensities for reflections after 11° 2θ for Al-fum-(DMSO), in comparison to the activated Al-fum. The enhancement is induced by DMSO inside the pores of Al-fum(DMSO) which contributes to the scattering. This behavior was already observed by Thoma et al. for incorporated DMSO in NH_2-MIL-53(Al).[33,34] The broadening of the reflections for both Al-fum and Al-fum(DMSO), in comparison to the simulated pattern, is due to the small crystallite size.[35,36] Following the Scherrer equation (eq 5) the crystallite size from the (0 1 1) reflection at 2θ = 10.45° was calculated to 20 nm. Note that the crystallite size is not comparable to the particle size, as particles can be made up of several different crystallites or crystallite domains or consist of a crystalline and amorphous fraction.

Besides the morphology, other crucial characteristics for the synthesized MOF, used as a filler for MMMs, are sorption properties of the very compound. Recent studies of Kanehashi et al. showed a linear dependence between the gas permeability and the fractional free volume (FFV) of the MMMs.[21] Therefore, Brunauer, Emmett, Teller (BET) surface area and pore volume for Al-fum and Al-fum(DMSO) were determined from a nitrogen sorption isotherm at 77 K (Figure 2). Al-fum

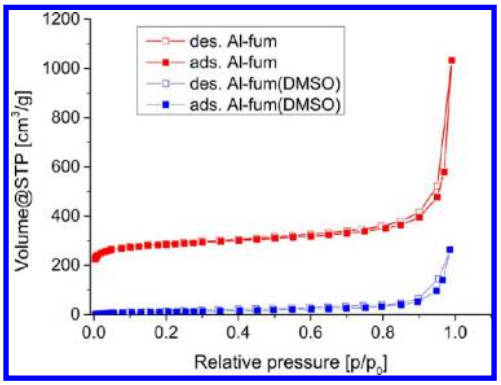

Figure 2. Nitrogen sorption isotherms of Al-fum (red) and Al-fum(DMSO) (blue) at 77 K.

shows as a first approximation a Type I nitrogen adsorption isotherm, typical for microporous materials,[38] yielding a BET surface area of 1100 m^2 g^{-1} and a total pore volume of 0.47 cm^3 g^{-1}. The micropore volume, given by the V-t-plot method according to DeBoer, is 0.37 cm^3 g^{-1}. For comparison BET surfaces areas and pore volumes of several Al-fum literature reports are collected in Table S1.

In contrast Al-fum(DMSO) shows no nitrogen uptake upon low relative pressures, hence displays no micropore volume. The calculated BET surface area of Al-fum(DMSO) of 40 m^2 g^{-1} represents primarily the external surface area due to the small particle size of the MOF. Both N_2 sorption isotherms for Al-fum and Al-fum(DMSO) show a continuous slight increase in gas uptake above p/p_0 = 0.4 with increasing relative pressure. A strong rise in gas uptake above p/p_0 = 0.9 gives the isotherms a Type II or Type III isotherm appearance and high nitrogen uptake for both compounds toward the saturation pressure (i.e., at p/p_0 = 1). This curvature can be explained by interparticle condensation in the macropores formed by the particle aggregates, which is showing here because of the intentionally prepared submicrometer particles.[39,40] Al-fum samples of larger particle size, porous or nonporous (DMSO-filled), do not show this continuous gas uptake with increasing relative pressure (Figure S3 in the SI). Hence, the MOF-pore volume determination must be limited to the MOF-inherent micro- and mesoporosity. A comparison of Figures 2 and S3 in SI shows that at p/p_0 > 0.4 the interparticle volume between submicrometer particles and concomitant pore condensation leads to a nitrogen uptake, which would then include this external volume. We decided to take the total pore volume at p/p_0 = 0.4 in order not to overestimate the micro- and mesopore volume inside the framework.

IR spectra of Al-fum(DMSO) showed an additional peak which can be assigned to the stretching vibration of the sulfur−oxygen double bond (1040−1060 cm^{-1}) (Figure S4).

Thermogravimetric analysis (TGA) and elemental analysis were conducted to determine the exact amount and ratio of the loaded DMSO to the MOF.

From TGA (Figure 3), Al-fum exhibits its typical degradation at around 400 °C with a mass loss of 59%

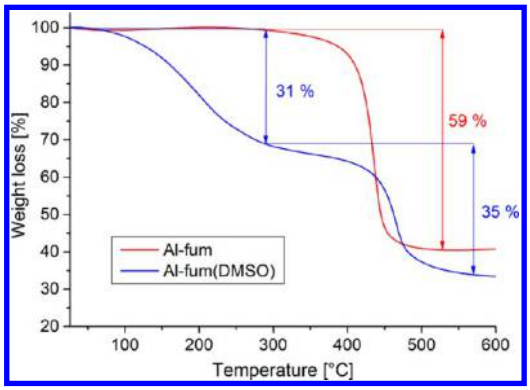

Figure 3. Thermogravimetric analysis (TGA) curves of Al-fum (red) and Al-fum(DMSO) (blue) under synthetic air at a heating flow of 2 K/min.

associated with the decay of the organic linker. In comparison Al-fum(DMSO) shows a continuous mass loss of 31% from 100 °C to 280 °C, where the Al-fum material starts to degrade, followed by the mass loss for the linker decay. The presence and loss of 0.31 g DMSO per g Al-fum(DMSO) with 0.69 g Al-fum sample correlates with a liquid DMSO density of 1.1 g/cm^3, hence the volume of 0.28 cm^3 in the pore volume of 0.47 cm^3/g × 0.69 g = 0.32 cm^3. Since the continuous mass loss occurs after thorough drying at 1 × 10^{-3} mbar at room temperature, it can be attributed to the desorption of DMSO from inside the pores other than just free solvent. The mass ratio of 0.31 g DMSO and 0.69 g Al-fum yields a molar ratio of approximately 0.8:1. Elemental analysis for Al-fum and Al-fum(DMSO) are represented in Table S2 and show a ratio of about 0.8:1 for DMSO to Al-fum. The slight difference in calculated and experimental elemental analysis can result from water retained in DMSO or in the MOF itself, which is in good agreement with the higher amount of hydrogen and the fewer amount of sulfur in comparison to the calculated value for both samples.

The porous filler material of MMMs is usually thought to contribute to the gas separation properties of the MMMs and could even enhance the selectivity of the MMMs compared to the neat polymer membrane.[41,42] Here the separation of CO_2 and CH_4 is used to test for this effect (Figure S5). The gas uptake in the porous Al-fum for CO_2 and CH_4 at 870 mmHg was 3.8 mmol/g and 1.4 mmol/g, respectively. The selectivity of 3.98 was obtained by the Henry plots of the adsorption isotherms (Figure S6) and is in good agreement with the

DOI: 10.1021/acsami.8b12938
ACS Appl. Mater. Interfaces 2018, 10, 33589−33600

literature for gas adsorptions measurements with a neat microsized Al-fum powder.[43] Note that the value of the selectivity for single-gas adsorption has little to do with the selectivity for neat or mixed-matrix membranes made from this MOF.[44,45]

Membrane Preparation and Gas Permeation Experiments. For the MMMs Matrimid 5218 (Figure 4) was chosen as a polymer due to its high thermal and chemical stability as well as its widespread implementation in MMMs so far. Matrimid has shown good interaction capability with MOFs as filler materials caused by polar carbonyl and imide groups which can interact with the MOF crystallites.[46,47]

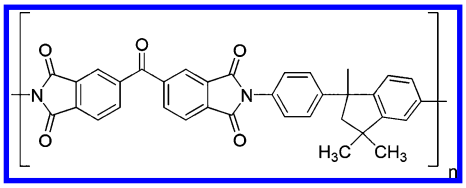

Figure 4. Structure of Matrimid.

All MMMs were prepared in the same procedure using a priming protocol in combination with multiple ultrasonication steps to receive uniform dispersed MOF particles in the polymer matrix. To determine the MOF particle distribution and embedment in the MMMs, SEM images of the cross sections in combination with an energy-dispersive X-ray spectroscopic (EDX) mapping of aluminum and sulfur were realized.

Figure 5 shows typical SEM images of cross sections for MMMs of Al-fum/Matrimid MMMs with different MOF loadings, prepared by freeze fracturing. The SEM images together with EDX depict an excellent particle distribution throughout all membranes. Close-up images of the cross section endorse a good compatibility between MOF and polymer, marked by no significant interfacial void formation around the filler particles.

EDX mapping of aluminum confirms homogeneous distribution of the filler despite minor sedimentation for various MMMs with different MOF loadings, shown by locally increased intensity of the mapped aluminum (Figure 6). Most important is to point out that even with higher loadings of Al-fum, the sedimentation of the filler remains in a reasonable scope and therefore uniformly homogeneous, dense MMMs are formed.

In the same manner MMMs of Al-fum(DMSO)/Matrimid were analyzed. Overviews and close-ups of the cross section of MMMs loaded with 4 and 24 wt % Al-fum(DSMO) are shown in Figure 7. They show equally good particle distribution across the whole MMMs. Close-up images are rather similar to the MMMs of Al-fum/Matrimid MMMs and show no interfacial void formation around the filler particles and the polymer. Figure 8 displays EDX-mapping of aluminum in red and sulfur in blue of the same cross sections shown in Figure 7. Aluminum as well as sulfur are detected homogeneously throughout the MMMs and in a similar intensity, which indicates a uniform distribution and high loading of DMSO in the pores of Al-fum. Moreover, EDX-mapping reveals minimal sedimentation for MMMs with 24 wt % MOF.

Mixed gas permeation experiments were carried out from a 50:50 v:v CO_2/CH_4 mixture at 25 °C and a transmembrane pressure of 3 bar. CO_2 and CH_4 gas permeabilities of the neat polymer and Al-fum/Matrimid MMMs are presented in Table S5 and Figure 9.

In general gas permeability increases with the increase of Al-fum loading. The selectivity increases slightly up to a loading of 20 wt %. Only for a loading of 24 wt % the selectivity drops again due to emerging microdefects, like agglomeration of MOF particles, resulting in connected nonselective voids between polymer and MOF or MOF particles themselves.[23] The 24 wt % membrane is also mechanically sensitive and quite brittle. Al-fum/Matrimid MMMs with 20 wt % performed the best with an improvement of 63% in CO_2 permeation and 28% in selectivity compared to the neat polymer. The observed trend of higher MOF loading resulting in an increased permeability is intrinsic for porous fillers in MMMs and is frequently observed.[48−50] The gas permeability and selectivity enhancement can be traced back to improved gas diffusivity and adsorption of the MMMs. Diffusivity is either influenced by the free fractional volume (FFV) of the polymer and the MOF or by interfacial voids between polymer and MOF (void volume).[21,28] The influence of both FFV and void volume is discussed in a following section. Adsorption properties of Al-fum affect the selectivity of MMMs in a desired way. The adsorption properties of Al-fum with a near 4:1 selectivity of CO_2 over CH_4, calculated from the initial Henry plot of the CO_2 and CH_4 adsorption isotherms (Figures S5 and S6), cause an improvement of selectivity with increasing MOF loading. Due to its quadrupole moment CO_2 is more likely to interact and adsorb on Al-fum causing its superior selectivity of CO_2 over CH_4.

Likewise mixed gas permeation experiments with Al-fum(DMSO)/Matrimid MMMs were carried out. The results are presented in Table S6 and in Figure 10. An Al:S quantification of the Al-fum(DMSO)/Matrimid MMMs before and after the gas permeation studies gave the same molar ratio within experimental error (Tables S3 and S4 in the SI). This ensured that no DMSO was removed upon gas permeation, hence, the nonporous nature of Al-fum(DMSO) was retained.

For the membrane with the nonporous Al-fum(DMSO) filler both CO_2 and CH_4 permeabilities are reduced in similar proportion with increased loading of Al-fum(DMSO). Consequently, the selectivity stays largely constant for the different MMM loadings. CO_2 permeabilities decrease constantly from about 6.6 Barrer of the neat polymer to 5.0 Barrer in the MMMs with 24 wt % MOF loading (24% reduction). Equally CH_4 permeability reduces from 0.14 Barrer to 0.10 Barrer (28% reduction), respectively. As described in the Introduction, compared to the effect of porous fillers, nonporous fillers have shown diverse impacts in MMMs. Either nonporous fillers increase the permeability while mostly reducing the selectivity due to the formation of defects,[25] or to the contrary nonporous fillers lead to a decrease in permeability while retaining the selectivity of the polymer.[28,51] In this work the latter is observed, which emerges out of the nature of the used filler. Usually inorganic oxides were used as nonporous fillers, showing poor interactions with most polymers. MOFs on the other hand are known to develop favorable interactions with the polymer, which leads to fewer microdefects in the MMMs. Therefore, it is not surprising that MMMs consisting of nonporous Al-fum(DMSO) and Matrimid show a reduction in permeability with increasing filler loading, as the FFV of the MOF is essentially zero and the volume of the polymer is constantly reduced.

DOI: 10.1021/acsami.8b12938
ACS Appl. Mater. Interfaces 2018, 10, 33589−33600

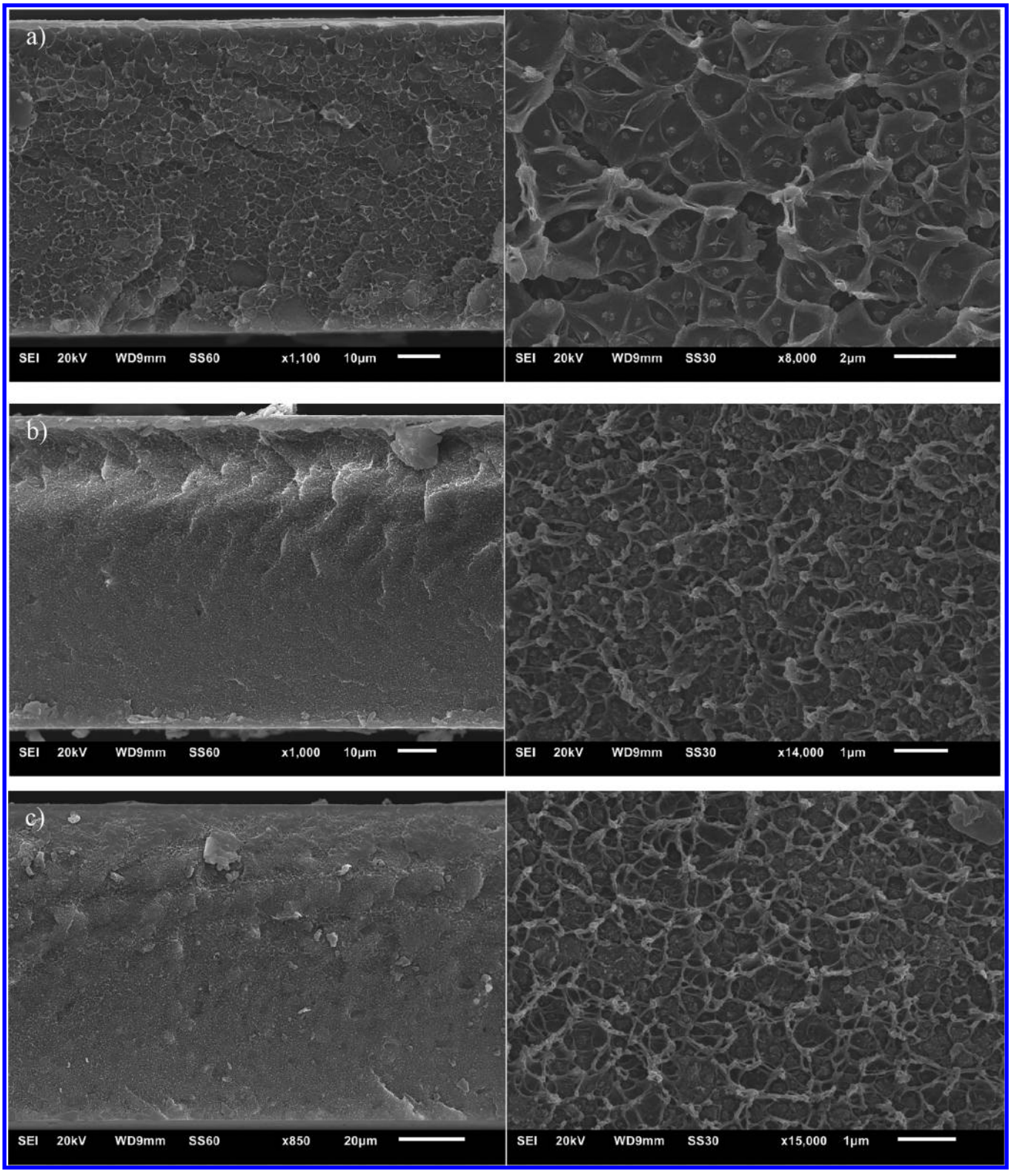

Figure 5. SEM images of cross section of Matrimid with different loadings of Al-fum as filler a) 8 wt %, b) 16 wt %, and c) 24 wt %.

Modeling of Gas Permeation. *Maxwell Model.* The Maxwell model can be applied to both porous and nonporous fillers in composite membranes to predict the permeability of the composite membrane. Prior works have shown poor or only qualitative trend agreements for porous and nonporous fillers compared to the predicted values of the Maxwell model.[51−54] The values for the observed permeability could often not be reproduced with the model. The discrepancy between model and experiment can result from stronger deviations between assumptions and reality, for example, for particle geometry, dispersion, or maximum filler loading, which are essential for the model, or the unaccounted presence of microdefects due to poor interaction between filler and polymer. Figure 11 shows the comparison between predicted

DOI: 10.1021/acsami.8b12938
ACS Appl. Mater. Interfaces 2018, 10, 33589−33600

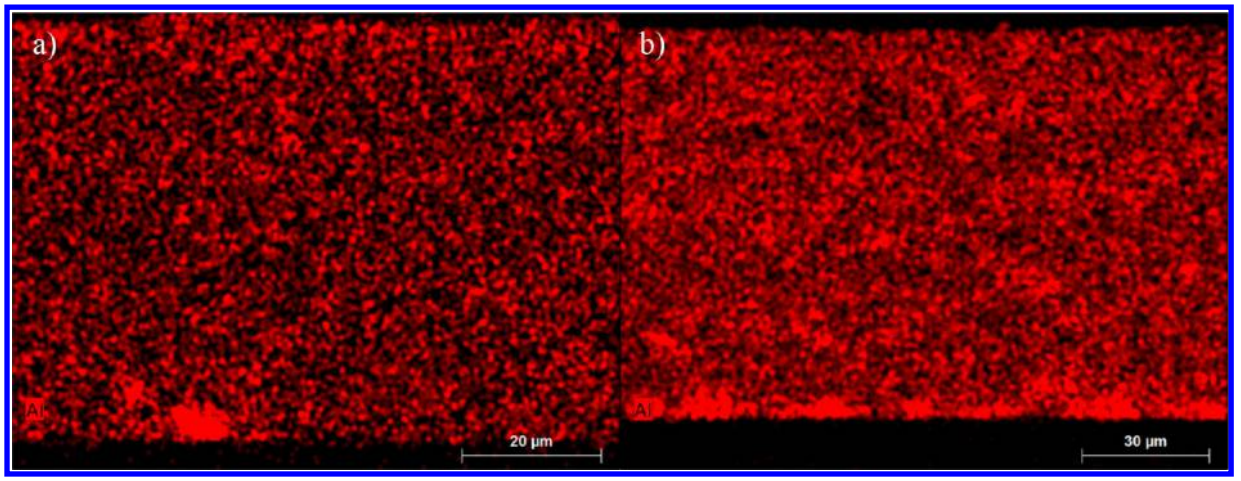

Figure 6. EDX-mapping of aluminum (red) in MMM cross sections of a) 4 wt % Al-fum and b) 24 wt % Al-fum. The bottom of the images corresponds to the bottom of the membrane when casted.

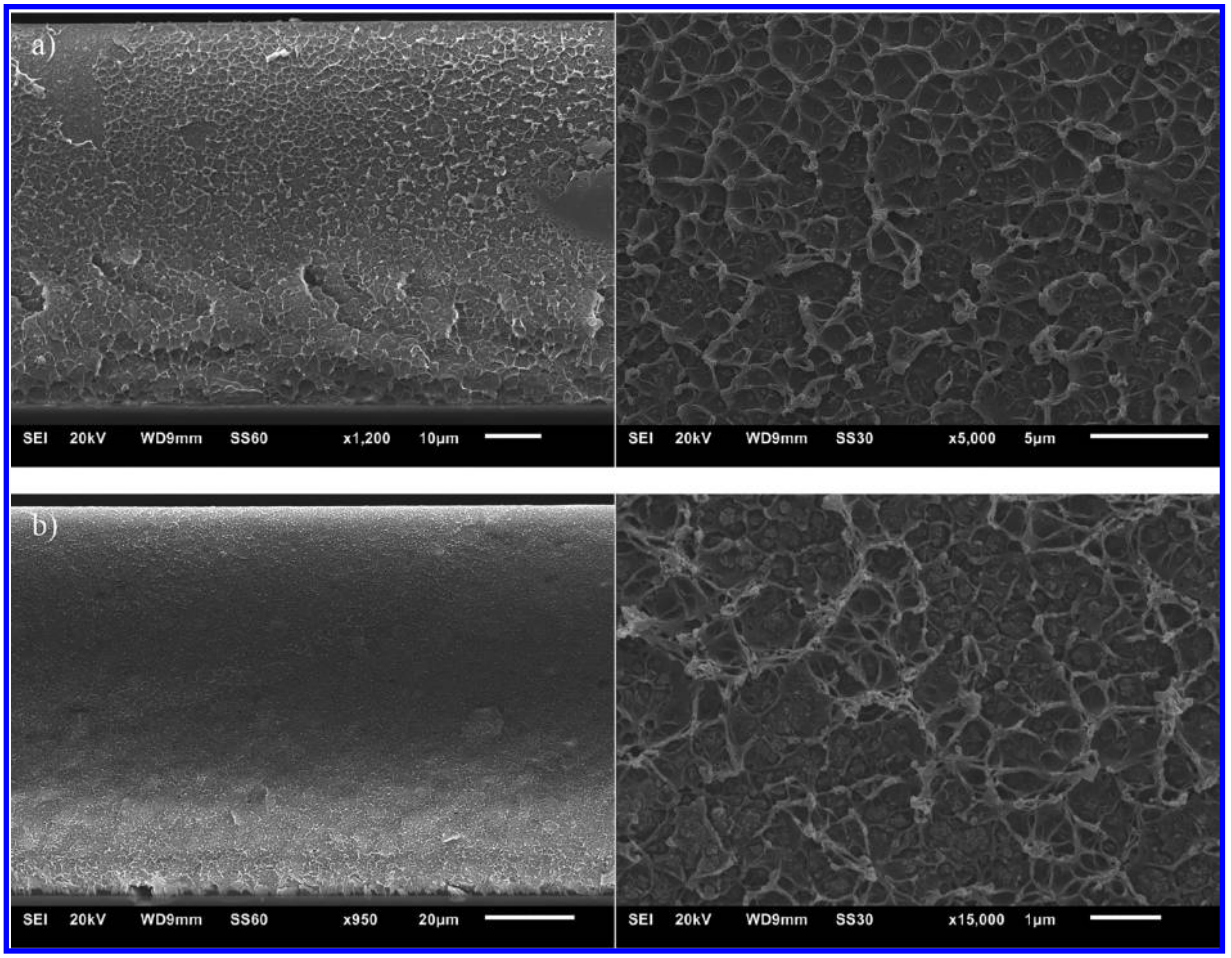

Figure 7. SEM images of cross-section of Matrimid with different loadings of Al-fum(DMSO) as filler a) 4 wt %, b) 24 wt %.

(Maxwell model) and experimental relative CO_2 permeabilities for MOF−Matrimid composite membranes with porous Al-fum and nonporous Al-fum(DMSO) fillers.

Relative experimental CO_2 permeabilities for Al-fum/Matrimid MMMs are in good agreement with the theoretical values from the Maxwell model for porous fillers ($P_d \gg P_c$). The reduction of the relative experimental CO_2 permeability for Al-fum(DMSO)/Matrimid MMMs is a good indicator for homogeneous dispersed filler particle and good interactions between polymer and MOF. Otherwise interparticular, non-selective voids should result in increased permeabilities and reduced selectivity.

Similarly, the relative CH_4 permeabilities were plotted against the filler volume in Figure S7. For CH_4 the experimental permeabilities also follow the theoretical prediction albeit with a slightly larger deviation than for CO_2.

Free Fractional Volume (FFV). In the literature, the (total) FFV was defined as the sum of the volume-weighted specific

DOI: 10.1021/acsami.8b12938
ACS Appl. Mater. Interfaces 2018, 10, 33589−33600

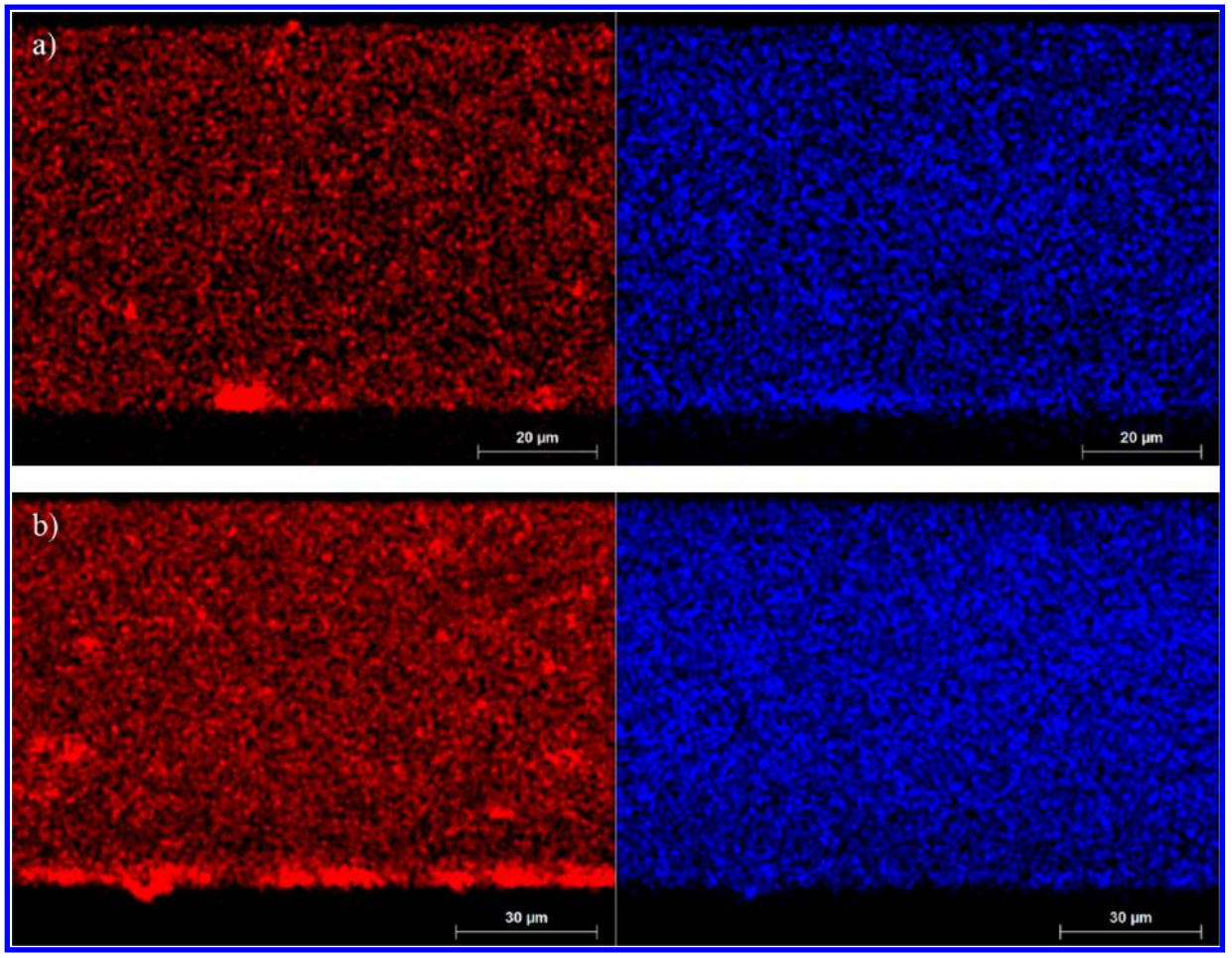

Figure 8. EDX-mapping of aluminum (red) and sulfur (blue) in MMM cross sections of a) 4 wt % Al-fum(DMSO) and b) 24 wt % Al-fum(DMSO). The molar Al:S quantification in Al-fum(DMSO) by EDX spectroscopy is given in Tables S3 and S4.

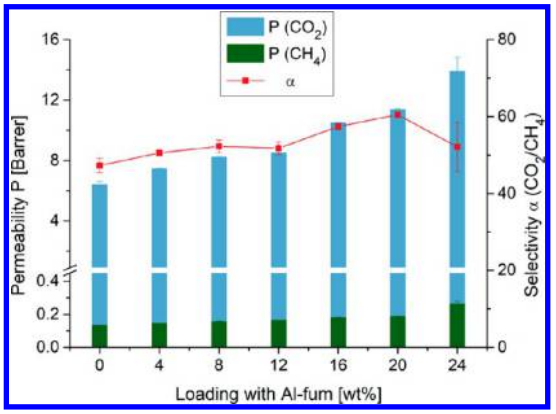

Figure 9. Performance of Al-fum/Matrimid MMMs with different Al-fum loadings in the separation of CO_2 and CH_4. The 24 wt % membrane was prepared and measured four times to ensure reproducibility and significance of the selectivity drop.

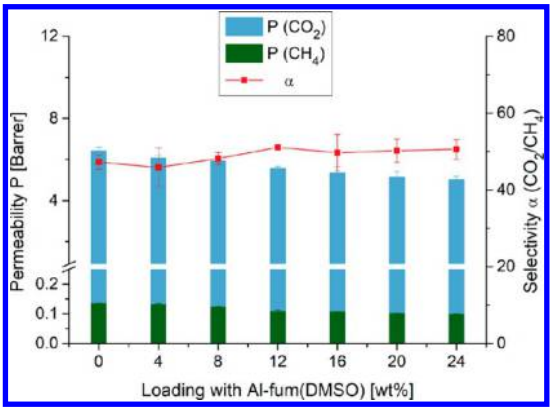

Figure 10. Performance of Al-fum(DMSO)/Matrimid MMMs with different Al-fum loadings in the separation of CO_2 and CH_4.

pore volumes (in cm^3/g) multiplied with the specific densities (in g/cm^3) of the materials (polymer, filler) in the MMM. Thereby, the FFV became a dimensionless entity (see Section S10 in the SI). Multiplication of pore volume with density was done to allow for comparison of the correlated permeability for different fillers.[21]

Here we want to elucidate the possible relative role of the FFV of the polymer, the MOF, and the void volume of the MOF−polymer interface. Therefore, we need to elucidate and compare actual specific free volumes (in units cm^3/g).

Thus, we define here a (total) specific free fractional volume sFFV as the sum of the volume-weighted (ϕ_c, ϕ_d) specific free volumes (sFV) of the polymer and the filler (eq 1). The sFV of the neat polymer Matrimid (density 1.167 g/cm^3) was reported to approximately 0.146 cm^3/g.[21,55] The sFV of the MOF is usually taken as equal to the total specific pore volume V_p determined by nitrogen sorption (Table S1).[21]

DOI: 10.1021/acsami.8b12938
ACS Appl. Mater. Interfaces 2018, 10, 33589−33600

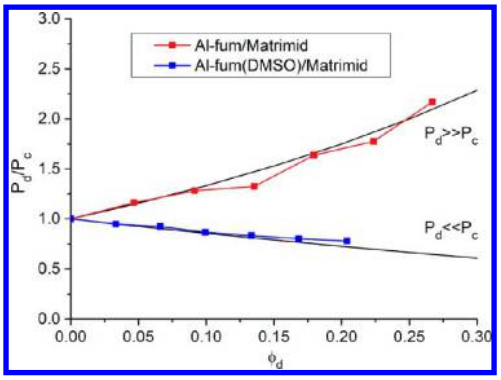

Figure 11. Relative experimental CO_2 permeabilities (referenced to the permeability P_c of the pure polymer membrane) for Al-fum/Matrimid (red curve) and Al-fum(DMSO)/MMMs (blue curve) with different filler volume fraction ϕ_d. The black lines give the relative theoretical CO_2 permeabilities for porous (filler permeability $P_d \gg P_c$) and nonporous ($P_d \ll P_c$) fillers. Note that for the same wt % of MOF the higher density of nonporous Al-fum(DMSO) leads to a lower filler volume fraction.

$$\text{(total) sFFV} = \text{sFV}_{\text{polymer}} \times \phi_c + \text{sFV}_{\text{MOF}} \times \phi_d \quad (1)$$

A listing of the sFFV values for the MMMs with different filler fractions is given in Table S7 and Table S8 in the SI. The sFFV ranges from 0.23 cm^3/g for a 24 wt % Al-fum/Matrimid MMM to 0.12 cm^3/g for a 24 wt % Al-fum(DMSO)/Matrimid MMM.

The FFV includes only the porosity in the polymer and filler and does not include any voids formed around the filler particles due to phase incompatibility. For the FFV the correlation with permeability P is given by the following:

$$P = A_p \times \exp^{(-B_p/\text{FFV})} \quad (2)$$

which is linearized to

$$\lg P = \lg A_p - \frac{B_p}{2.303\text{FFV}} \quad (3)$$

with A_p and B_p being gas- and temperature-dependent constants.[56]

Thus, if indeed the FFV determines the permeability a plot of lg P versus 1/FFV should give a straight line with slope $-B_p/2.303$ and intercept lg A_p.

A plot of lg P versus the inverse of the specific free fractional volume sFFV, is given in Figure 12 for the two gases CO_2 and CH_4 which were tested with the porous and nonporous Al-fum/Matrimid MMMs.

The plot of lg P versus 1/sFFV shows for both gases a very good linear correlation over the Al-fum and Al-fum(DMSO)/Matrimid MMMs. As the sFFV rises with decreasing nonporous Al-fum(DMSO) filler and increasing filler volume of porous Al-fum, the inverse sFFV decreases.

This illustrates that the sFFV is not only applicable for composite membranes with porous fillers, but is also usable for composite membranes with nonporous fillers. The values for A_p and B_p, calculated from the linear regression of the lg P versus 1/sFFV (1/FFV) plot (Figures 12 and S12), are presented in Table S9 (SI). Similar to previous studies the values for B_p are relatively similar for CO_2 and CH_4 for both FFV and sFFV. A_p values differ highly between CO_2 to CH_4 which is also in good agreement with the literature.[56,57] The difference in A_p, in unit Barrer, could be a result of the smaller

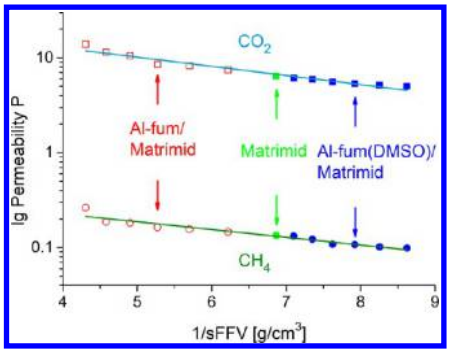

Figure 12. Combined experimental CO_2 and CH_4 permeabilities of porous and nonporous Al-fum and Al-fum(DMSO)/Matrimid MMMs as a function of the inverse (total) specific free fractional volume, sFFV. The neat polymer Matrimid has 1/sFFV = 6.9, the 24 wt % Al-fum/MMM 4.3, and the 24 wt % Alfum(DMSO)/MMM has 8.6. The straight lines are only intended as a guide to the eye.

kinetic diameter of CO_2 (3.3 Å) compared to CH_4 (3.8 Å) which leads to a faster motion within the free volume of the polymer lamellar and MOF. Furthermore, CO_2 is more likely to get adsorbed in the MOF and therefore may travel faster through the fractional free volume introduced by the MOF.

Void Volume (VV). Besides the sFFV, which focuses on the free volume inside the polymer and the MOF, one can likewise determine the interface volume (void volume) between the polymer and the embedded MOF particles and its impact on the gas permeability. Takahashi and Paul showed that excess free volume between polymer and silica filler particles can lead to an increase in permeability, even for nonporous fillers due to poor interactions of the inorganic nanoparticles with the polymer phase and contrary to the Maxwell model. They obtained the excess void volume from a lower measured density than the theoretically determined one.[28,29] Further they described various possible morphologies of interparticular voids in composite membranes and acknowledged that the effect of the voids will be highly dependent on their distribution throughout the system.

In the literature, the void volume was derived from the difference between theoretical (D_{theo}) and measured density (D_{exp}) of the MMM according to ($[1 - D_{\text{exp}}/D_{\text{theo}}] \times 100\%$). Thereby, the void volume became a dimensionless entity.[23,29] As we want to elucidate the relative role of the FFV of the polymer, the MOF and the void volume of the MOF−polymer interface, we need to elucidate and compare actual specific free and void volumes (in units cm^3/g).

The possible specific void volume (sVV) between continuous and dispersed phase is determined according to eq 4:

$$\text{specific void volume, sVV} = \frac{1}{D_{\text{exp}}} - \frac{1}{D_{\text{theo}}} \quad (4)$$

The results for the specific void volume determination of Al-fum/Matrimid MMMs are depicted in Figure 13.

The deviation in theoretical and measured density is very small and mostly within the error bar. Thus, none of the MMMs show significant specific void volume formation. Overall there is no apparent trend for an increasing void volume formation with increasing filler volume observed. This is in contrast to the continuous rise of the permeability with increasing filler volume for the composite membranes. Hence,

DOI: 10.1021/acsami.8b12938
ACS Appl. Mater. Interfaces 2018, 10, 33589−33600

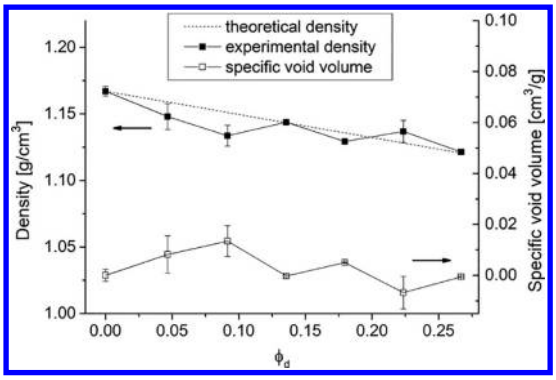

Figure 13. Specific void volume (eq 4) for Al-fum/Matrimid MMMs with different filler volumes. MMMs with 24 wt % MOF were no longer included in the presentation.

the void volume seems to have at most only a slight influence on the performance of the prepared MMMs.

Similar results for Al-fum(DMSO)/Matrimid MMMs are shown in Figure 14. The overall void volume is approximately

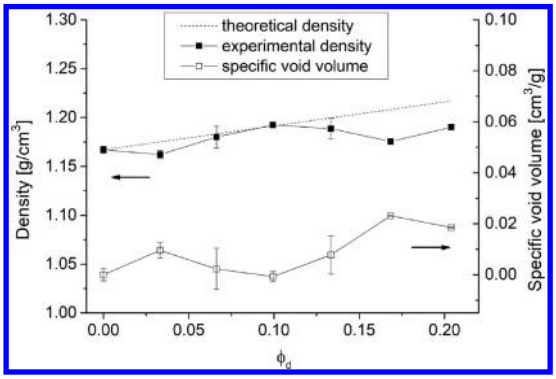

Figure 14. Specific void volume (eq 4) derived by the difference between theoretical and measured density for Al-fum(DMSO)/Matrimid MMMs with different filler volumes.

the same as for the MMMs with the porous filler, but this time there might be a trend to higher specific void volume formation for MMMs with higher filler volumes. But since the CO_2 and CH_4 permeability for Al-fum(DMSO)/Matrimid MMMs decreases with higher MOF loadings (Table S6) there clearly is no correlation between void volume formation and separation performance in this case.

CONCLUSIONS

In this work porous, submicrometer sized Al-fum was synthesized according to the literature.[30] Nonporous Al-fum(DMSO) was obtained by heating Al-fum in DMSO and characterized with various methods. Both porous and nonporous aluminum fumarate fillers were embedded in a Matrimid matrix, thereby leading to the same polymer−filler interface. SEM images in combination with EDX-mapping revealed a mostly homogeneous filler distribution throughout all MMMs. CO_2/CH_4 separation performances showed reverse effects for porous and nonporous fillers. MMMs with the porous filler showed a continuous increase in CO_2 and CH_4 permeability while MMMs with the nonporous filler displayed a decrease in CO_2 and CH_4 permeability with rising filler content. These results are in good agreement with the Maxwell model, which predicts an increase in gas permeability for porous fillers and a decrease for nonporous fillers, respectively. The increase and decrease in gas permeability in general seems to be traceable to the difference in FFV, that is, the increased and decreased free volume of the polymer and filler. The interfacial void volume between filler and polymer contributes roughly only 10% to the available free volume in the MMM. This is most obvious regarding the gas permeation results of the MMMs with the nonporous filler compared to the measured void volume. Despite a constant to slightly growing void volume for higher nonporous filler loadings the gas permeabilities decrease. This clearly shows the negligible effect of an interfacial volume, both in absolute as in relative terms to the FFV. The organic/inorganic hybrid nature of the MOF filler certainly allowed for good compatibility with the polymer which is crucial to obtain defect free MMMs. As the free fractional volume, introduced by both the polymer and the MOF is decisive for the permeability both materials should be chosen accordingly. An increase in permeability requires high free volumes in both polymer and MOF. Thus, for MOFs a high pore volume is decisive for high permeable MMMs. In comparison to other porous fillers like zeolites MOFs should not only be advantageous because of their better compatibilities with organic polymers but also because of their higher pore volumes. Furthermore, a loss of linearity between FFV and permeability in MMMs would be a good indicator for an insufficient compatibility of the MOF and polymer which then probably results in void volume formation, with rise in permeability and partial loss of selectivity.

EXPERIMENTAL SECTION

Materials and Methods. All starting materials and solvents were obtained from commercial sources and used without further purification unless otherwise mentioned in the experimental description. Sodium aluminate (calculated as Al_2O_3 50−56%) was received from VWR chemicals, fumaric acid (99%) was obtained from TCI, dichloromethane (99%), *N*,*N*-dimethylformamide (99.99%) and dimethyl sulfoxide (99%) were purchased from Fisher Chemicals. Ethanol (99.99%) was obtained from Sigma-Aldrich. The polymer Matrimid 5218 was kindly supplied by Huntsman Advanced Materials.

Aluminum fumarate was synthesized according to the literature with the aim to obtain particles around 250 nm in size.[30] In a 100 mL round-bottom flask 0.45 g (5.49 mmol) of sodium aluminate and 0.9 g (7.76 mmol) of fumaric acid were dissolved in 50 mL of water and heated in a 90 °C preheated water bath for 30 min. After cooling down to room temperature the precipitate was collected by filtration and washed with water and ethanol for 1 day each. The collected product was dried at 150 °C in vacuum (50 mbar) overnight (yield 0.81 g, 94% based on sodium aluminate). The product was positively characterized as the MOF aluminum fumarate by powder X-ray diffraction, thermogravimetric analysis, and nitrogen sorption measurements as is detailed in the Results and Discussion.

Aluminum fumarate(DMSO) was synthesized by suspending 0.8 g aluminum fumarate in 100 mL dimethyl sulfoxide and then refluxed at 180 °C bath temperature overnight. The product was collected by filtration and dried at room temperature in vacuum (1×10^{-3} mbar) for 24 h. The pore filling and the amount of DMSO was determined by thermogravimetric analysis and elemental analysis as is detailed in the Results and Discussion.

Matrimid was dried at 80 °C for several days to remove the adsorbed moisture. All MMMs were prepared using a prime protocol to reduce agglomeration of the MOF particles and ensure a successful preparation. In the following the procedure for MMMs with 4 wt % MOF is described as an example of all prepared MMMs. The amount of 0.4 g of Matrimid was dissolved in 3.5 mL of dichloromethane and stirred for 24 h. At the same time 17 mg of the MOF was suspended

DOI: 10.1021/acsami.8b12938
ACS Appl. Mater. Interfaces 2018, 10, 33589−33600

in 4.5 mL of dichloromethane and also stirred for 24 h. Then the MOF suspension was ultrasonicated three times for 15 min with an amplitude of 20% at an ultrasonic liquid processor (VCX 750 Sonics, Microtip 630−0419) to homogenize the suspension. Between the ultrasonication steps, the suspension was stirred for 30 min. Afterward 0.16 mL of the polymer solution were added to the MOF suspension to receive an equal polymer/MOF mass ratio. After another 24 h of stirring and the same homogenization procedure, the remaining polymer was added to the MOF/polymer mixture and stirred further for 1 h. Afterward this mixture was casted into a metal ring, which was placed on a flat glass plate. To ensure slow evaporation of the solvent and to protect the membranes from dust the metal rings were immediately covered with inverted funnels. The membranes were left to dry for 3 h at room temperature and then taken off the glass plate by immersing in water and afterward dried at 150 °C overnight in the vacuum oven (50 mbar). The MMMs with 8, 12, 16, 20, 24 wt % MOF were prepared in the same way with 35 mg, 54.5 mg, 76 mg, 100 mg, and 126.5 mg MOF, respectively. The added polymer solution was adapted as follows: 0.33 mL, 0.52 mL, 0.72 mL, 0.95 mL, and 1.20 mL, respectively.

Powder X-ray diffraction (PXRD) patterns were obtained on a Bruker D2 Phaser powder diffractometer equipped with a flat silicon, low background sample holder using Cu−K_α radiation (λ = 1.5418 Å, 30 kV, 10 Ma, ambient temperature). With this sample holder at $2\theta <$ ~10° the beam spot is strongly broadened so that only a fraction of the reflected radiation reaches the detector; hence lower relative intensities are measured in this range. All samples were measured with a scan speed of 2s/step and a step size of 0.028° (2θ). Simulated patterns of aluminum fumarate were calculated with CCDC Mercury 3.9 program using the single crystal data of Basolite A520 obtained by Rietveld refinement (CCDC no. 1051975, Refcode DOYBEA).[37] The Bruker D2 Phaser had been calibrated with an LaB_6 NIST standard sample of known crystallite size (0.8 μm) for calculating the Al-fum crystallite size with the Scherrer equation (eq 5). The full width at half-maximum ($\Delta(2\theta)$) of the reflexes depends inversely on the crystallite size (L), which results in broadened reflexes for small crystallite sizes as seen in Figure 1.

$$\Delta(2\theta) = \frac{K \times \lambda}{L \times \cos(\theta_0)} \tag{5}$$

SEM images were recorded with a Jeol JSM-6510LV QSEM Advanced electron microscope with a LAB-6 cathode at 20 keV. The microscope was equipped with a Bruker Xflash 410 silicon drift detector and the Bruker ESPRIT software for EDX analysis. The membrane cross sections were prepared through freeze-fracturing after immersion in liquid nitrogen and then coated with gold by a Jeol JFC 1200 fine-coater at an approximate current of 20 mA for 20−30 s.

Thermogravimetric analysis (TGA) were carried out with a Netzsch TG 209 F3 Tarsus in the range of 25 °C to 600 °C with a heating rate of 2 K min^{-1} under oxygen atmosphere.

Infrared (IR) spectra were obtained with a Bruker FT-IR Tensor 37 as attenuated total reflection. The scanning frequency range was 4000−500 cm^{-1}.

Nitrogen sorption measurements at 77 K were carried out on a Quantachrome NOVA 4000e gas sorption analyzer and evaluated with the AsiQwin V3 software. For activation the sample was degassed in a vacuum of 5 × 10^{-2} mbar at 150 °C for 3 h. The Brunauer−Emmett−Teller (BET) surface areas were calculated in the p/p_0-range of 0.01−0.05. Total pore volumes were calculated from nitrogen adsorptions isotherms at p/p_0 = 0.4. Micropore analysis was done with DeBoer thickness method via V-t-Plot method in the pressure range of p/p_0 0.25−0.5 of the adsorption isotherm. Adsorption isotherms for aluminum fumarate with CO_2 and CH_4 were recorded on a Micromeritics ASAP 2020 gas sorption analyzer equipped with oil-free vacuum pumps and valves, which guaranteed contamination free measurements. CO_2 and CH_4 isotherms were measured at 0 °C (ice/deionized water bath). All gases were of ultrapure grades (99.999%) supplied by Air Liquide Germany and used as-received.

Binary gas separation experiments were performed with a continuous flow permeation system (OSMO inspector, provided by Convergence Industry B.V., 7532 SM Enschede, The Netherlands) with helium as sweep gas and an Agilent 490 μGC gas chromatograph to measure the gas concentration in the permeate. The membranes were cut in a round sheet, placed in the permeation module (4.5 cm diameter) and covered by a rubber mask to provide an effective inner diameter of 3.6 cm with an area of 11.3 cm^2. All permeation experiments were conducted at 25 °C and with 3 bar transmembrane pressure. The feed gases were mixed in a 50/50 volume flow mixture of CO_2 and CH_4 by two Bronkhorst Coriolis-flow controllers as well as the helium gas stream with a total upstream flow of 160 mL min^{-1}. The downstream is swept with helium at a rate of 1 mL min^{-1} at ambient pressure. The gas concentration in the permeate stream was measured with an Agilent 490 μ gas chromatograph with thermal conductivity detector and a Pora PLOT Q column every 30 min until steady state (up to 8 h). Each membrane sample was produced twice to ensure reproducibility. Permeability of the membranes was calculated according to the following equation:

$$P_A = \frac{x_{1A} \times S_{Fl} \times d}{x^p_{He} \times A \times (p_2 \times x_{2A} - p_1 \times x_{1A})} \tag{6}$$

where P_A is the permeability of the gas A in Barrer (1 Barrer = 10^{-10}·cm^3(STP)cm/(cm^2·s·cmHg)), x_{1A} the molar fraction of the gas A, S_{Fl} the flow of the sweep gas in cm^3 s^{-1}, d the thickness of the membrane, x^p_{He} the molar fraction of the sweep gas in the permeate, A the membrane area in cm^2, x_{2A} the molar fraction of the gas A in the feed and p_1, and p_2 the permeate and feed pressure in cmHg, respectively. The error bars in the permselectivity diagrams mark the range of values obtained from the independent measurement of two membranes.

Density (ρ) of the membranes was determined by measuring their volume and mass (eq 8). The membranes were measured 3 times on an analytical balance (d = 0.1 mg) to receive the mean mass. The volume (V) was derived with the formula of a cylindric body (eq 7). Both diameter ($2r$) and thickness (h) were measured at 10 different sites to receive an average diameter and thickness.

$$V = \pi \times r^2 \times h \tag{7}$$

$$\rho = \frac{\text{mass}}{\text{volume}} \tag{8}$$

Equations for the gas transport in polymeric membranes and the Maxwell model are given Section S12 in the SI.

■ ASSOCIATED CONTENT

Supporting Information

The Supporting Information is available free of charge on the ACS Publications website at DOI: 10.1021/acsami.8b12938.

Structure description of aluminum fumarate, SEM images of aluminum fumarate and aluminum fumarate-(DMSO); additional N_2 sorption isotherms of micrometer sized aluminum fumarate particles; IR spectra and elemental analysis of both compounds; Al:S quantification of various MMMs by EDX spectroscopy; CO_2 and CH_4 sorption of aluminum fumarate; gas separation performances of all MMMs; relative experimental CH_4 permeabilities compared to the Maxwell model; additional theoretical and experimental properties of all MMMs regarding the FFV, sFFV, and void volume; and equations for the gas transport in polymeric membranes and the Maxwell model (PDF)

DOI: 10.1021/acsami.8b12938
ACS Appl. Mater. Interfaces 2018, 10, 33589−33600

AUTHOR INFORMATION

Corresponding Author

*Tel.: +49 211 81 12286. Fax: +49 211 81 12287. E-mail: janiak@hhu.de (C.J.).

ORCID

Christoph Janiak: 0000-0002-6288-9605

Notes

The authors declare no competing financial interest.

ACKNOWLEDGMENTS

The authors acknowledge the financial support of the Federal German Ministry of Education and Research (BMBF) in the project Optimat under grant no. 03SF0492C. We thank Mrs. Alexa Schmitz and Mr. Moritz Steinert for the thermogravimetric analyses.

ABBREVIATIONS

Al-fum = aluminum fumarate
DMSO = dimethyl sulfoxide
FVV = free fractional volume
fum = fumarate
MMM = mixed-matrix membrane
MOF = metal−organic framework
VV = void volume

REFERENCES

(1) Bernardo, P.; Drioli, E.; Golemme, G. Membrane Gas Seperation: A review/State of the Art. *Ind. Eng. Chem. Res.* **2009**, *48*, 4638−4663.

(2) Moulijn, J. A.; Makkee, M.; van Diepen, A. *Chemical Process Technology*; John Wiley & Sons: Chichester, England, 2001.

(3) Tobin, J.; Shambaugh, P.; Mastrangelo, E. *Energy Information Administration, Office of Oil and Gas*, January 2006. http://www.dnr.louisiana.gov/assets/docs/oilgas/naturalgas/ngprocess_20060131.pdf (assessed July 30, 2018).

(4) Davis, J. C.; Valus, R. J.; Eshraghi, R.; Velikoff, A. E. Facilitated Transport Membrane Hybrid Systems for Olefin Purification. *Sep. Sci. Technol.* **1993**, *28*, 463−476.

(5) Koros, W. J.; Mahajan, R. J. Pushing the limits on possibilities for large-scale gas separation: which strategies? *J. Membr. Sci.* **2000**, *175*, 181−196.

(6) Coronas, J.; Santamaría, J. Separations Using Zeolite Membranes. *Sep. Purif. Methods* **1999**, *28*, 127−177.

(7) Baker, R. W. Future Directions of Membrane Gas Separation Technology. *Ind. Eng. Chem. Res.* **2002**, *41*, 1393−1411.

(8) Koros, W. J.; Fleming, G. K. Membran-based gas separation. *J. Membr. Sci.* **1993**, *83*, 1−80.

(9) Robeson, L. M. Correlation of separation factor versus permeability for polymeric membranes. *J. Membr. Sci.* **1991**, *62*, 165−185.

(10) Robeson, L. M. The upper bound revisited. *J. Membr. Sci.* **2008**, *320*, 390−400.

(11) Zimmerman, C. M.; Singh, A.; Koros, W. J. Tailoring mixed matrix composite membranes for gas separations. *J. Membr. Sci.* **1997**, *137*, 145−154.

(12) Tanh Jeazet, H. B.; Staudt, C.; Janiak, C. Metal-organic frameworks in mixed-matrix membranes for gas separation. *Dalton Trans* **2012**, *41*, 14003−14027.

(13) Zornoza, B.; Martinez-Joaristi, A.; Serra-Crespo, P.; Tellez, C.; Coronas, J.; Gascon, J.; Kapteijn, F. Functionalized flexible MOFs as fillers in mixed matrix membranes for highly selective separation of CO_2 from CH4 at elevated pressures. *Chem. Commun.* **2011**, *47*, 9522−9524.

(14) Merkel, T. C.; Freeman, B. D.; Spontak, R. J.; He, Z.; Pinnau, I.; Meakin, P.; Hill, A. J. Ultrapermeable, reverse-selective nanocomposite membranes. *Science* **2002**, *296*, 519−522.

(15) Caro, J.; Noack, M. Zeolite membranes − Recent developments and progress. *Microporous Mesoporous Mater.* **2008**, *115*, 215−233.

(16) Zornoza, B.; Tellez, C.; Coronas, J.; Gascon, J.; Kapteijn, F. Metal organic framework based mixed matrix membranes: An increasingly important field of research with a large application potential. *Microporous Mesoporous Mater.* **2013**, *166*, 67−78.

(17) Kosinov, N.; Gascon, J.; Kapteijn, F.; Hensen, E. J. M. Recent developments in zeolite membranes for gas separation. *J. Membr. Sci.* **2016**, *499*, 65−79.

(18) Sorribas, S.; Zornoza, B.; Téllez, C.; Coronas, J. Mixed matrix membranes comprising silica-(ZIF-8) core−shell spheres with ordered meso−microporosity for natural- and bio-gas upgrading. *J. Membr. Sci.* **2014**, *452*, 184−192.

(19) Furukawa, H.; Cordova, K. E.; O'Keeffe, M.; Yaghi, O. M. The chemistry and applications of metal-organic frameworks. *Science* **2013**, *341*, 1230444.

(20) Dechnik, J.; Sumby, C. J.; Janiak, C. Enhancing Mixed-Matrix Membrane Performance with Metal−Organic Framework Additives. *Cryst. Growth Des.* **2017**, *17*, 4467−4488.

(21) Kanehashi, S.; Chen, G. Q.; Scholes, C. A.; Ozcelik, B.; Hua, C.; Ciddor, L.; Southon, P. D.; D'Alessandro, D. M.; Kentish, S. E. Enhancing gas permeability in mixed matrix membranes through tuning the nanoparticle properties. *J. Membr. Sci.* **2015**, *482*, 49−55.

(22) Dong, G.; Li, H.; Chen, V. Challenges and opportunities for mixed-matrix membranes for gas separation. *J. Mater. Chem. A* **2013**, *1*, 4610−4630.

(23) Takahashi, S.; Paul, D. R. Gas permeation in poly(ether imide) nanocomposite membranes based on surface-treated silica. Part 1: Without chemical coupling to matrix. *Polymer* **2006**, *47*, 7519−7534.

(24) Zhang, Y.; Feng, X.; Yuan, S.; Zhou, J.; Wang, B. Challenges and recent advances in MOF−polymer composite membranes for gas separation. *Inorg. Chem. Front.* **2016**, *3*, 896−909.

(25) Basu, S.; Cano-Odena, A.; Vankelecom, I. F. J. MOF-containing mixed-matrix membranes for CO_2/CH_4 and CO_2/N_2 binary gas mixture separations. *Sep. Purif. Technol.* **2011**, *81*, 31−40.

(26) Ahmadpour, E.; Sarfaraz, M. V.; Behbahani, R. M.; Shamsabadi, A. A.; Aghajani, M. Fabrication of mixed matrix membranes containing TiO2 nanoparticles in Pebax 1657 as a copolymer on an ultra-porous PVC support. *J. Nat. Gas Sci. Eng.* **2016**, *35*, 33−41.

(27) Sadeghi, M.; Semsarzadeh, M. A.; Barikani, M.; Pourafshari Chenar, M. Gas separation properties of polyether-based polyurethane−silica nanocomposite membranes. *J. Membr. Sci.* **2011**, *376*, 188−195.

(28) Ahn, J.; Chung, W.-J.; Pinnau, I.; Guiver, M. D. Polysulfone/silica nanoparticle mixed-matrix membranes for gas separation. *J. Membr. Sci.* **2008**, *314*, 123−133.

(29) Takahashi, S.; Paul, D. R. Gas permeation in poly(ether imide) nanocomposite membranes based on surface-treated silica. Part 2: With chemical coupling to matrix. *Polymer* **2006**, *47*, 7535−7547.

(30) Zhou, L.; Zhang, X.; Chen, Y. Facile synthesis of Al-fumarate metal−organic framework nano-flakes and their highly selective adsorption of volatile organic compounds. *Mater. Lett.* **2017**, *197*, 224−227.

(31) Dechnik, J.; Nuhnen, A.; Janiak, C. Mixed-Matrix Membranes of the Air-Stable MOF-5 Analogue [Co4(μ4-O)(Me2pzba)3] with a Mixed-Functional Pyrazolate-Carboxylate Linker for CO_2/CH_4 Separation. *Cryst. Growth Des.* **2017**, *17*, 4090−4099.

(32) Sabetghadam, A.; Seoane, B.; Keskin, D.; Duim, N.; Rodenas, T.; Shahid, S.; Sorribas, S.; Le Guillouzer, C.; Clet, G.; Tellez, C.; Daturi, M.; Coronas, J.; Kapteijn, F.; Gascon, J. Metal Organic Framework Crystals in Mixed-Matrix Membranes: Impact of the Filler Morphology on the Gas Separation Performance. *Adv. Funct. Mater.* **2016**, *26*, 3154−3163.

(33) Thoma, R.; Kärger, J.; de Sousa Amadeu, N.; Niessing, S.; Janiak, C. Assessing Guest-Molecule Diffusion in Heterogeneous Powder Samples of Metal-Organic Frameworks through Pulsed-Field-

DOI: 10.1021/acsami.8b12938
ACS Appl. Mater. Interfaces 2018, 10, 33589−33600

Gradient (PFG) NMR Spectroscopy. *Chem. - Eur. J.* **2017**, *23*, 13000−13005.
(34) Glomb, S.; Woschko, D.; Makhloufi, G.; Janiak, C. Metal-Organic Frameworks with Internal Urea-Functionalized Dicarboxylate Linkers for SO_2 and NH_3 Adsorption. *ACS Appl. Mater. Interfaces* **2017**, *9*, 37419−37434.
(35) Loiseau, T.; Serre, C.; Huguenard, C.; Fink, G.; Taulelle, F.; Henry, M.; Bataille, T.; Ferey, G. A rationale for the large breathing of the porous aluminum terephthalate (MIL-53) upon hydration. *Chem. - Eur. J.* **2004**, *10*, 1373−1382.
(36) Gaab, M.; Trukhan, N.; Maurer, S.; Gummaraju, R.; Müller, U. The progression of Al-based metal-organic frameworks − From academic research to industrial production and applications. *Microporous Mesoporous Mater.* **2012**, *157*, 131−136.
(37) Alvarez, E.; Guillou, N.; Martineau, C.; Bueken, B.; Van de Voorde, B.; Le Guillouzer, C.; Fabry, P.; Nouar, F.; Taulelle, F.; de Vos, D.; Chang, J. S.; Cho, K. H.; Ramsahye, N.; Devic, T.; Daturi, M.; Maurin, G.; Serre, C. The structure of the aluminum fumarate metal-organic framework A520. *Angew. Chem., Int. Ed.* **2015**, *54*, 3664−3668.
(38) Thommes, M.; Kaneko, K.; Neimark, A. V.; Olivier, J. P.; Rodriguez-Reinoso, F.; Rouquerol, J.; Sing, K. S. W. Physisorption of gases, with special reference to the evaluation of surface area and pore size distribution (IUPAC Technical Report). *Pure Appl. Chem.* **2015**, *87*, 1051−1069.
(39) Jiang, D.; Burrows, A. D.; Edler, K. J. Size-controlled synthesis of MIL-101(Cr) nanoparticles with enhanced selectivity for CO_2 over N_2. *CrystEngComm* **2011**, *13*, 6916−6919.
(40) Zamidi Ahmad, M.; Navarro, M.; Lhotka, M.; Zornoza, B.; Téllez, C.; Fila, V.; Coronas, J. Enhancement of CO 2 /CH 4 separation performances of 6FDA-based co-polyimides mixed matrix membranes embedded with UiO-66 nanoparticles. *Sep. Purif. Technol.* **2018**, *192*, 465−474.
(41) Yang, S.; Sun, J.; Ramirez-Cuesta, A. J.; Callear, S. K.; David, W. I.; Anderson, D. P.; Newby, R.; Blake, A. J.; Parker, J. E.; Tang, C. C.; Schroder, M. Selectivity and direct visualization of carbon dioxide and sulfur dioxide in a decorated porous host. *Nat. Chem.* **2012**, *4*, 887−894.
(42) Jacques, N. M.; Rought, P. R. E.; Fritsch, D.; Savage, M.; Godfrey, H. G. W.; Li, L.; Mitra, T.; Frogley, M. D.; Cinque, G.; Yang, S.; Schroder, M. Locating the binding domains in a highly selective mixed matrix membrane via synchrotron IR microspectroscopy. *Chem. Commun.* **2018**, *54*, 2866−2869.
(43) Rubio-Martinez, M.; Leong, T.; Juliano, P.; Hadley, T. D.; Batten, M. P.; Polyzos, A.; Lim, K.-S.; Hill, M. R. Scalable simultaneous activation and separation of metal−organic frameworks. *RSC Adv.* **2016**, *6*, 5523−5527.
(44) Bux, H.; Liang, F.; Li, Y.; Cravillon, J.; Wiebcke, M.; Caro, J. Zeolitic Imidazolate Framework Membrane with Molecular Sieving Properties by Microwave-Assisted Solvothermal Synthesis. *J. Am. Chem. Soc.* **2009**, *131*, 16000−16001.
(45) Guo, H.; Zhu, G.; Hewitt, I. J.; Qiu, S. Twin Copper Source Growth of Metal-Organic Framework Membrane: $Cu_3(BTC)_2$ with High Permeability and Selectivity for Recycling H_2. *J. Am. Chem. Soc.* **2009**, *131*, 1646−1647.
(46) Hwang, S.; Chi, W. S.; Lee, S. J.; Im, S. H.; Kim, J. H.; Kim, J. Hollow ZIF-8 nanoparticles improve the permeability of mixed matrix membranes for CO2/CH4 gas separation. *J. Membr. Sci.* **2015**, *480*, 11−19.
(47) Venna, S. R.; Lartey, M.; Li, T.; Spore, A.; Kumar, S.; Nulwala, H. B.; Luebke, D. R.; Rosi, N. L.; Albenze, E. Fabrication of MMMs with improved gas separation properties using externally-functionalized MOF particles. *J. Mater. Chem. A* **2015**, *3*, 5014−5022.
(48) Ordoñez, M. J. C.; Balkus, K. J.; Ferraris, J. P.; Musselman, I. H. Molecular sieving realized with ZIF-8/Matrimid® mixed-matrix membranes. *J. Membr. Sci.* **2010**, *361*, 28−37.
(49) Zhang, Y.; Musselman, I. H.; Ferraris, J. P.; Balkus, K. J. Gas permeability properties of Matrimid® membranes containing the metal-organic framework Cu−BPY−HFS. *J. Membr. Sci.* **2008**, *313*, 170−181.
(50) Etxeberria-Benavides, M.; David, O.; Johnson, T.; Łozińska, M. M.; Orsi, A.; Wright, P. A.; Mastel, S.; Hillenbrand, R.; Kapteijn, F.; Gascon, J. High performance mixed matrix membranes (MMMs) composed of ZIF-94 filler and 6FDA-DAM polymer. *J. Membr. Sci.* **2018**, *550*, 198−207.
(51) Shen, Y.; Lua, A. C. Theoretical and experimental studies on the gas transport properties of mixed matrix membranes based on polyvinylidene fluoride. *AIChE J.* **2013**, *59*, 4715−4726.
(52) Rafiq, S.; Maulud, A.; Man, Z.; Mutalib, M. I. A.; Ahmad, F.; Khan, A. U.; Khan, A. L.; Ghauri, M.; Muhammad, N. Modelling in mixed matrix membranes for gas separation. *Can. J. Chem. Eng.* **2015**, *93*, 88−95.
(53) Sadeghi, Z.; Omidkhah, M.; Masoumi, M. E.; Abedini, R. Modification of existing permeation models of mixed matrix membranes filled with porous particles for gas separation. *Can. J. Chem. Eng.* **2016**, *94*, 547−555.
(54) Jeazet, H. B.; Koschine, T.; Staudt, C.; Raetzke, K.; Janiak, C. Correlation of Gas Permeability in a Metal-Organic Framework MIL-101(Cr)-Polysulfone Mixed-Matrix Membrane with Free Volume Measurements by Positron Annihilation Lifetime Spectroscopy (PALS). *Membranes (Basel, Switz.)* **2013**, *3*, 331−353.
(55) Huang, Y.; Wang, X.; Paul, D. Physical aging of thin glassy polymer films: Free volume interpretation. *J. Membr. Sci.* **2006**, *277*, 219−229.
(56) Kanehashi, S.; Nagai, K. Analysis of dual-mode model parameters for gas sorption in glassy polymers. *J. Membr. Sci.* **2005**, *253*, 117−138.
(57) Park, J. Y.; Paul, D. R. Correlation and prediction of gas permeability in glassy polymer membrane materials via a modified free volume based group contribution method. *J. Membr. Sci.* **1997**, *125*, 23−39.

DOI: 10.1021/acsami.8b12938
ACS Appl. Mater. Interfaces 2018, 10, 33589−33600